Molecular dynamics simulation of structural and dynamic properties of selenium structures with different degrees of amorphization

C Oligschleger, C Facius, H Kutz, C Langen, M Thumm,
S von Brühl, S Wang, L Weber and J Zischler

FB Angewandte Naturwissenschaften, HS Bonn-Rhein-Sieg, von-Liebig-Straße 20,
53359 Rheinbach, Germany

Abstract

We investigated Se structures of different degrees of disorder ranging from a 5% up to a 95% degree of amorphization. Starting from a trigonal crystalline structure we applied different strategies to introduce disorder into the Se configurations by irradiating atoms from their crystalline equilibrium positions. According to the symmetry of the trigonal phase, we introduced three types of disorder, i.e. the first type where only atoms forming layers of complete helical chains are shifted from their original positions (the thickness of these layers is chosen to represent the chosen degree of amorphicity), the second type where only atoms in planes—of respective thicknesses—lying perpendicular to the chains are displaced and the third type where only randomly chosen atoms are shifted from their crystalline equilibrium positions. After a thermal treatment of these disordered starting configurations, we calculated structural and dynamic properties (i.e. pair-correlation function and vibrational spectrum) and compared the results to both the original crystalline data and results obtained from corresponding glass structures.

1. Introduction

Due to their disorder glasses and amorphous materials possess properties which differ strongly from their crystalline counterparts [1]. At low temperatures thermal conductivity of an amorphous material is orders of magnitude smaller compared to the crystalline modifications and specific heat in disordered matter is much higher than in the crystals, respectively. The aim of our simulations is to investigate structural and dynamic properties of materials with different degrees of amorphization. Both ceramics and glasses belong to the class of (solid) disordered materials in which the glasses undergo a so-called melting route—and therefore are often referred to as undercooled liquids—in which the crystalline starting material is heated to temperatures well above the melting point, equilibrated and subsequently quenched at high rates below the glass transition temperature T_g. Since the performance of even massively parallel computers is limited in both memory and speed, the molecular dynamics (MD)

simulation of atomic or molecular systems is confined to so-called large scale systems (which are still orders of magnitude smaller compared to real experimental samples) [2, 3] and, due to the necessarily small molecular dynamics integration time step, long simulation times are excluded [4]. These small observation periods are also the reason for the high quenching rates (typical values are at least $\dot{Q} = 10^{12}$ K s^{-1} and several orders of magnitude larger than the experimental ones [5]) applied during the MD melting route. In order to avoid the unphysical high quenching rates, efforts have been undertaken to apply other processes to introduce disorder into Se structures, e.g. evaporation studies [6, 7]. To shorten this long procedure of the melting route and to show the equivalence of disordered structures—at least for some structural and dynamic properties—we propose an irradiation of the crystalline structure which also gives an insight into different types of defects/degrees of disorder which will be reflected by the anisotropic properties. Another advantage of the irradiation (which means that a fraction of atoms—

1

Table 1. Parameters of equations (2) and (5) for the radial parts of the two- and three-body interactions. The values of the parameters are given in au.

Two-body potential	Three-body-potential
$r \leqslant r_p = 1.6$	$r \leqslant r_p = 1.6$
$a_1 = 9281.2$	$c_1 = 8.8297$
$a_2 = 0.268\,02$	$c_2 = -2.5932$
$a_3 = -16.599$	$c_3 = -6.9384$
$\alpha_1 = -7.9284$	$\gamma_1 = -0.476\,01$
$\alpha_2 = -7.7781 \times 10^{-5}$	$\gamma_2 = -1.5637$
$\alpha_3 = -1.8634$	$\gamma_3 = -0.370\,49$
$r_p < r \leqslant r_c = 2.37$	$r_p < r \leqslant r_{c_3} = 2.35$
$b_1 = 1.864\,25$	$d_1 = 0.225\,56$
$b_2 = 4.586\,28$	$d_2 = 0.125\,27$
$b_3 = 3.620\,29$	$d_3 = -0.210\,19$

according to the degree of amorphization—is chosen to be shifted from the crystalline positions) is a much shorter simulation time in comparison to the classic melting route (for which one typically uses several ns in order to produce one structure). Applying this process of irradiation (which may experimentally be seen as locally disturbing the original crystal by means of, for example, an incident ray of neutrons) one obtains better statistics in a similar computation time compared to the generation of one glass structure. The influence of disorder on properties is important for the design of special materials and will have an impact on the so-called tailored design. This is a field of continuous improvement for both practical applications and basic research. The thermodynamic and kinetic properties of material are ruled by, for example, low-frequency modes and the so-called Bose-peak which is shown to be dependent of the degree of amorphization [8], which is in the field of previous investigations where the focus is on the energetic development of the system under consideration, i.e. the relaxation of the structures [9–11]. This paper is organized as follows: in section 2 we give an overview of the model, used throughout the simulations and describe computational details. The results of structural and dynamic properties are presented in section 3, followed by a discussion and finally we summarize and give conclusive remarks.

2. Model, potential and computational details

Se exists in six experimentally known different crystalline allotropes (trigonal Se: under normal conditions the most stable phase is built from helical chains [12], α-, β- and γ-monoclinic selenium built from Se_8 molecules [12, 13] and a rhombohedric phase comprising Se_6 molecules [14]) and is known to be a strong glass former [15] which possesses localized modes [16, 17]. In our simulation we focus on the most stable structure, i.e. on the trigonal configuration and on amorphous structures based on irradiation of the crystalline phase.

The atomic interaction potential was fitted by Oligschleger *et al* [18] in order to reproduce structural and dynamic properties of Se molecules (based on experimental values [20–23] and on *ab initio* calculations [24] from [25–27]) and properties

of the crystalline phases [13, 28–31]. The potential consists of two-body and three-body-terms:

$$V = \sum_{i=1, j>i}^{N} v_2(r_{ij}) + \sum_{i=1, j>i, k>j}^{N} v_3(r_i, r_j, r_k). \quad (1)$$

The two-particle interaction contains only a short-range part smoothly cut off at 4.13 Å. The shape of the potential is similar to a Morse-type potential, and for computational convenience the two-body part is expressed by exponentials and given by

$$v_2(r) = \begin{cases} a_1 \exp(\alpha_1 r) + a_2 \exp(\alpha_2 r) \\ \quad + a_3 \exp(\alpha_3 r), & \text{with } r \leqslant r_p \\ b_1(r - r_c)^5 + b_2(r - r_c)^4 \\ \quad + b_3(r - r_c)^3, & \text{with } r_p < r \leqslant r_c \\ 0, & \text{with } r > r_c \end{cases} \quad (2)$$

with r being the distance between two interacting atoms.

The three-particle potential is cyclic and dependent only on distances (r_{ij}, between atoms i and j, and r_{kj}, between k and j) and angles (Θ_{ijk}, with j being the central atom). No distinction is made whether atoms are inter-chain or intra-chain neighbours. The functional form of the three-particle-term is a modified Stillinger–Weber-type [19]:

$$v_3(r_i, r_j, r_k) = h(r_{ij}, r_{kj}, \Theta_{ijk}) + \text{cycl.}, \quad (3)$$

where $h(r_{ij}, r_{kj}, \Theta_{ijk})$ is defined by

$$h(r_{ij}, r_{kj}, \Theta_{ijk}) = (\beta_1(\cos\Theta_{ijk} - \cos\beta_2)^2 + \beta_3 - 0.5\beta_1(\cos\Theta_{ijk})^4)u_3(r_{ij})u_3(r_{kj}) \quad (4)$$

with $\beta_1 = 34.486\,574$, $\beta_2 = 1.664\,494$ and $\beta_3 = 11.957\,231$. The radial part $u_3(r)$ is given by

$$u_3(r)$$
$$= \begin{cases} c_1 \exp(\gamma_1 r) + c_2 \exp(\gamma_2 r) \\ \quad + c_3 \exp(\gamma_3 r), & \text{with } r \leqslant r_p \\ d_1(r - r_{c_3})^5 + d_2(r - r_{c_3})^4 \\ \quad + d_3(r - r_{c_3})^3, & \text{with } r_p < r \leqslant r_{c_3} \\ 0, & \text{with } r > r_{c_3}. \end{cases} \quad (5)$$

All parameters are given in [18] and listed in table 1. In order to account for SI units, we use conversion factors for the distance (1 Å = 1.7426^{-1} au) and for the energy (1 eV = 3.2412^{-1} au) and the atomic weight for selenium is 78.96 atomic mass units.

Using trigonal Se as a well-known material for the preparation of disordered structures, seven degrees of amorphization (5%, 20%, 35%, 50%, 65%, 80% and 95%) are generated by shifting the respective number of atoms from their crystalline positions. The most stable Se configuration is the trigonal one (built up from parallel chains) and we used a crystalline starting configuration of 1470 atoms (70 chains with 21 atoms each). To introduce disorder into the crystalline starting configuration we followed three different strategies: (a) atoms within chains (which belong to a layer of a thickness corresponding to the chosen degree of amorphization) are shifted from their equilibrium

positions, (b) atoms lying in a plane perpendicular to the chains with a thickness corresponding to the chosen degree of amorphization are shifted from their equilibrium positions and (c) randomly chosen atoms (again the number of atoms is chosen corresponding to the desired degree of amorphization) are shifted from their equilibrium positions up to 0.06 Å. By means of these atomic displacements from the equilibrium positions, we apply additional potential energy to the system, which will react with relaxations in order to dissipate the local energy spot into other parts of the configuration.

With molecular dynamics (MD) one can simulate a variety of complex structures [32–36]. In order to determine structural, dynamic and thermodynamic quantities one typically explores correlation functions, e.g. determination of the van Hove correlation gives insight into the radial distribution of atomic distances, and the calculation of the velocity autocorrelation [37] or displacement autocorrelation [38] reveals the vibrational spectrum of configurations. After initially introducing disorder into the system, the structure is monitored for 10 000 molecular dynamics time steps (each 1.76 fs) with a velocity Verlet integration scheme at a temperature of 140 K, i.e. well below the glass transition temperature. We applied periodic boundary conditions to reduce surface effects and monitored the virial of the configuration to account for internal pressure. To improve statistics we generated ten configurations for each degree of disorder. A structural property which exhibits the crystalline or disordered status of matter is the so-called pair-correlation function $g(r)$:

$$g(r) = \left\langle \frac{n(r)}{4\pi r^2 \rho \Delta r} \right\rangle \qquad (6)$$

with $n(r)$ being the number of atoms at a distance r in a sphere with thickness Δr around a reference atom, ρ is the number density of atoms in the system and $\langle \ \rangle$ stands for averaging over configurations which are calculated throughout the molecular dynamics simulations.

After a final quench to 0 K by a steepest descent/conjugate gradient algorithm [39, 40] the minima of the potential hypersurface are identified which are used to calculate the dynamic matrix from which we determined the spectra of the disordered Se structures and calculated the participation ratio and the effective mass of the modes.

In order to measure the amorphicity of the structures we introduce the distance between the trigonal reference phase and the optimized configurations as quantifiable observables. The atomic displacements,

$$\Delta R^2 = \sum_n (\mathbf{R}_n^i - \mathbf{R}_n)^2, \qquad (7)$$

where $\mathbf{R}_n^i$ is the position vector of atom n in its position in a minimum i of the potential energy surface and $\mathbf{R}_n$ is the position of atom n in the trigonal Se crystal. The total displacement R which accounts for a structural change is given by $R = \sqrt{\Delta R^2}$ and measured in Å.

The harmonic vibrations of each glass configuration were calculated from the force constant matrix of the $T = 0$ K minimum configuration. The numerically exact minimization of the potential energy prevents the occurrence of spurious unstable modes. The elements of the force constant matrix are given by

$$D_{\alpha\beta}^{ij} = \frac{1}{\sqrt{m_i m_j}} \frac{\partial^2 V(|\mathbf{R}^i - \mathbf{R}^j|)}{\partial R_\alpha^i \partial R_\beta^j}. \qquad (8)$$

Here V is the potential energy (see equation (1)), the derivatives are with respect to the positions $\mathbf{R}^i$ and $\mathbf{R}^j$ of atoms i and j, and α and β stand for the Cartesian directions. Since we have only one type of atom, the masses m_i and m_j of atoms i and j are the same. Diagonalization of the dynamic matrix [41] yields both the eigenfrequencies as ω^2 and the eigenmodes using standard routines [42]. The frequency spectra are calculated from the frequencies of the $3N - 3$ vibrational modes [43] σ as

$$Z(\nu) = \left\langle \frac{1}{3N - 3} \sum_\sigma \delta(\nu - \nu^\sigma) \right\rangle, \qquad (9)$$

where δ is the discretized δ function and $\langle \ \rangle$ stands for the averaging over configurations. To measure frequency shifts in the vibrational spectra which give insight into the softening or hardening of vibrations or eigenmodes, we calculate the quantity $(\Delta \nu)^2$:

$$(\Delta \nu)^2 = \frac{1}{3N - 3} \sum_{\sigma=4}^{3N} (\nu(\sigma) - \nu_{\text{cryst}}(\sigma))^2 \qquad (10)$$

with $\nu(\sigma)$ being the eigenfrequency of mode σ of a disordered structure and $\nu_{\text{cryst}}(\sigma)$ being the eigenfrequency of mode σ of the crystalline structure, i.e. the trigonal configuration. Due to the translational invariance and periodic boundary conditions the first three eigenvalues are zero (and correspond to the three translational modes) and the sum is over all $3N - 3$ non-zero eigenfrequencies of the dynamic matrix and the corresponding spectrum (see equations (8) and (9)). Since we determine the square of the frequency shift, $(\Delta \nu)^2$ accounts for shifts to both lower and higher values of the frequencies.

Diagonalization of the force constant matrix, equation (8), also gives, besides the eigenvalues, the eigenvectors. These give the structures of the vibrations and can be used to determine, for example, the localization of the vibration. The localization of modes is typical for glassy states and at low frequency characteristic for the anomalous behaviour of disordered materials [17]. Usually there are two measures of localization, namely the effective mass and the participation ratio which both have been calculated in our present work. The effective mass is given in terms of the eigenvector as

$$m_{\text{eff}}(\nu) = m/|\mathbf{e}^1(\nu)|^2. \qquad (11)$$

Here we have assumed that the $3N$-dimensional unit vector of a mode with frequency ν is normalized and $\mathbf{e}^n(\nu)$ stands for the vector formed from the three components on atom n. Atom number 1 is taken as the atom with the largest displacement. $n_{\text{eff}} = m_{\text{eff}}/m$ is a measure for the number of atoms which effectively carry the kinetic energy of the vibrational mode. This definition is limited to small system sizes when the long-range tails of the modes are not too important. In the following

we will use mainly the participation ratio:

$$p(\nu) = \left(N \sum_{n=1}^{N} |\mathbf{e}^n(\nu)|^4 \right)^{-1}. \qquad (12)$$

For a translation one has $p = 1$ and for a vibration of a single atom with all others at rest $p = 1/N$. This scaling with $1/N$ should hold for all localized modes.

3. Results

The structures of 210 (i.e. seven degrees of amorphicity, three types of introducing disorder and ten models each) Se models are analysed with respect to the main structural information, namely the pair-correlation function, and the most important dynamic information, i.e. the vibrational frequency spectrum.

A first insight into the influence of the introduced disorder on properties is exemplified in figure 1. Here we give the results of structural models, pair-correlation function $g(r)$ and density of states $Z(\nu)$ for the trigonal phase shown in figure 1(a), three structural models of irradiated or disordered selenium given in figures 1(b)–(d) and a model of Se glass in figure 1(e). The amorphicity of the irradiated structures is introduced by shifting atoms in a plane—of a thickness corresponding to the degree of disorder—perpendicular to the chains. In figure 1(b) the model represent a structure with few structural defects (5% degree of disorder), while in figure 1(c) we present a structure of partial amorphization (35% degree of disorder) which exhibits already a clear separation between disordered and crystallized parts. In figure 1(d) we give an example of a completely disordered structure (95% degree of amorphization) which resembles all the features one would expect for glass structures shown in figure 1(e). All the irradiated structures were generated by introducing disorder within planes perpendicular to the chains; therefore the view is along the *a* axis. The pair-correlation function $g(r)$ is a good indication for the presence or absence of disorder within a structure. As can be seen from the pair-correlation function $g(r)$ for the crystallite configuration one can distinguish very sharp peaks from different neighbour shells. With increasing structural disorder we observe that in the corresponding pair-correlation functions a distinct decrease of the first neighbour peak occurs, i.e. broadening of the peak appears. Furthermore, the splitting of the next-nearest-neighbour peak in the pair-correlation function vanishes for a high degree of amorphicity and can only be found in structures with a reasonable amount of crystallinity. For dynamic properties we realize a similar pattern. Not only a strong decrease of individual peaks in the frequency spectra is observed with increasing disorder, but also a shift of the frequencies towards both lower and higher frequencies can be seen.

For better comparison we give the results for the trigonal structure (in figure 1(a)) and one glass configuration, see figure 1(e). At first the similarities between the pure crystalline structure and those with a low degree of disorder are striking: however, already the pair-correlation as well as the vibrational density of states exhibit (small) differences, and the broadening of the peaks in both $g(r)$ and $Z(\nu)$ reveals the presence of

impurities which break the symmetry of the structure. The structure with the highest degree of amorphization and those obtained via the melting route have similar results for both $g(r)$ and $Z(\nu)$. This is an indication of the fact that at least some properties of amorphous Se are independent of the method of production.

Since at high degrees of amorphicity the results are very similar and in good agreement with those obtained via the melting route, we would like to emphasize the effects of anisotropy in Se at low degrees of disorder. The various methods of irradiation exhibit a strong influence on different properties of the material, which on the other hand turn out heterogeneous reactions towards amorphicity and show varying sensitivities to defects and disorder. To envisage the differences between the methods applied in our simulations to introduce disorder into the structures it is helpful to have a closer look at representative configurations at a *low degree of amorphization*. The difference in the methods introducing disorder to selenium can be seen from figure 2 where we show a representative structure for the three methods applied, all having a degree of amorphicity of 20%. On the left side we present some starting configurations where those atoms shifted from their crystalline equilibrium positions are marked with green spheres, whereas the configurations, obtained after thermal treatment (MD at $T = 140$ K for 17.6 ps) and a final quench to 0 K, are plotted on the right side of the figure. In part (a) of figure 2 we show a structure where the disorder is generated within the chains and the view is along the *c* axis. In figure 2(b) we present a configuration which possesses disorder introduced into the plane, and in part (c) of figure 2 we give a representative configuration where the disorder is established with randomly chosen atoms and the view is along the *a* axis, respectively.

One structural criterion to measure the degree of disorder within a structure is the deviation (root mean square displacement) from its crystalline counterpart. This deviation is estimated by the calculation of the total displacements (which are given as the square roots of equation (7)). We use the structures after the final optimization procedure to calculate the displacements. The total displacements with respect to the crystalline trigonal structure are depicted in figure 3. In three graphs the displacements are plotted versus the degrees of amorphicity in order to distinguish between the different procedures applied to generate disorder. The graph of figure 3(a) shows the displacements of the structures where we introduced disorder within layers of chains, in figure 3(b) we present the results for the structures irradiated within planes, while at the bottom of the figure (figure 3(c)) one finds the displacements for structures having a randomly introduced amorphicity. For all types of irradiation the highest values of deviation from the trigonal reference configuration lie around 100–120 Å and are realized with already 65% disorder (taking the error bars into account). For the lowest degrees of amorphization one observes a linear increase of displacement with disorder (well expressed for the irradiation within planes perpendicular to the chains and those structures with disorder in layers of chains). Structures having randomly introduced disorder exhibit a rather high displacement from the trigonal
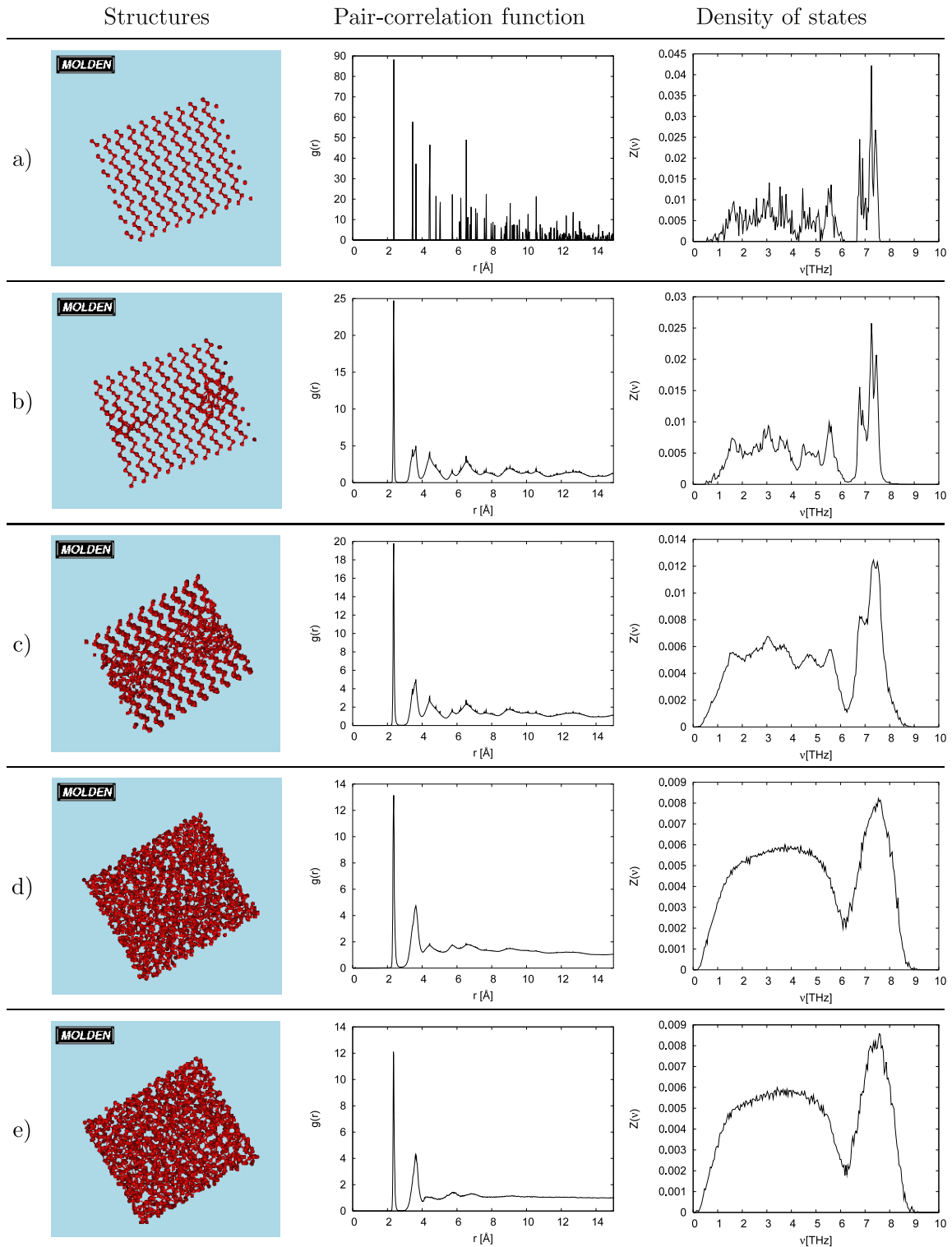
Figure 1. We present a representative structure, the pair-correlation function and density of states for (a) the trigonal phase, (b)–(d) three different degrees of amorphization (5%, 35% and 95%, respectively) by irradiation of atoms in a plane perpendicular to the chains and (e) an Se-glass structure.

structure at much lower degrees of amorphicity compared to the other methods.

To have a closer look at the influence on the structural properties we show in figure 4 the average pair-correlation function $g(r)$ plotted versus r obtained in the course of the molecular dynamics simulations. The different types of

amorphization strategies are plotted in individual sub-figures. For a better visualization we shifted the graphs of different degrees of disorder, and on the left side of each graph, we give the values of the corresponding degree of amorphization. For all types of disorder one can clearly see that for high degrees of amorphicity the same structural properties are obtained as
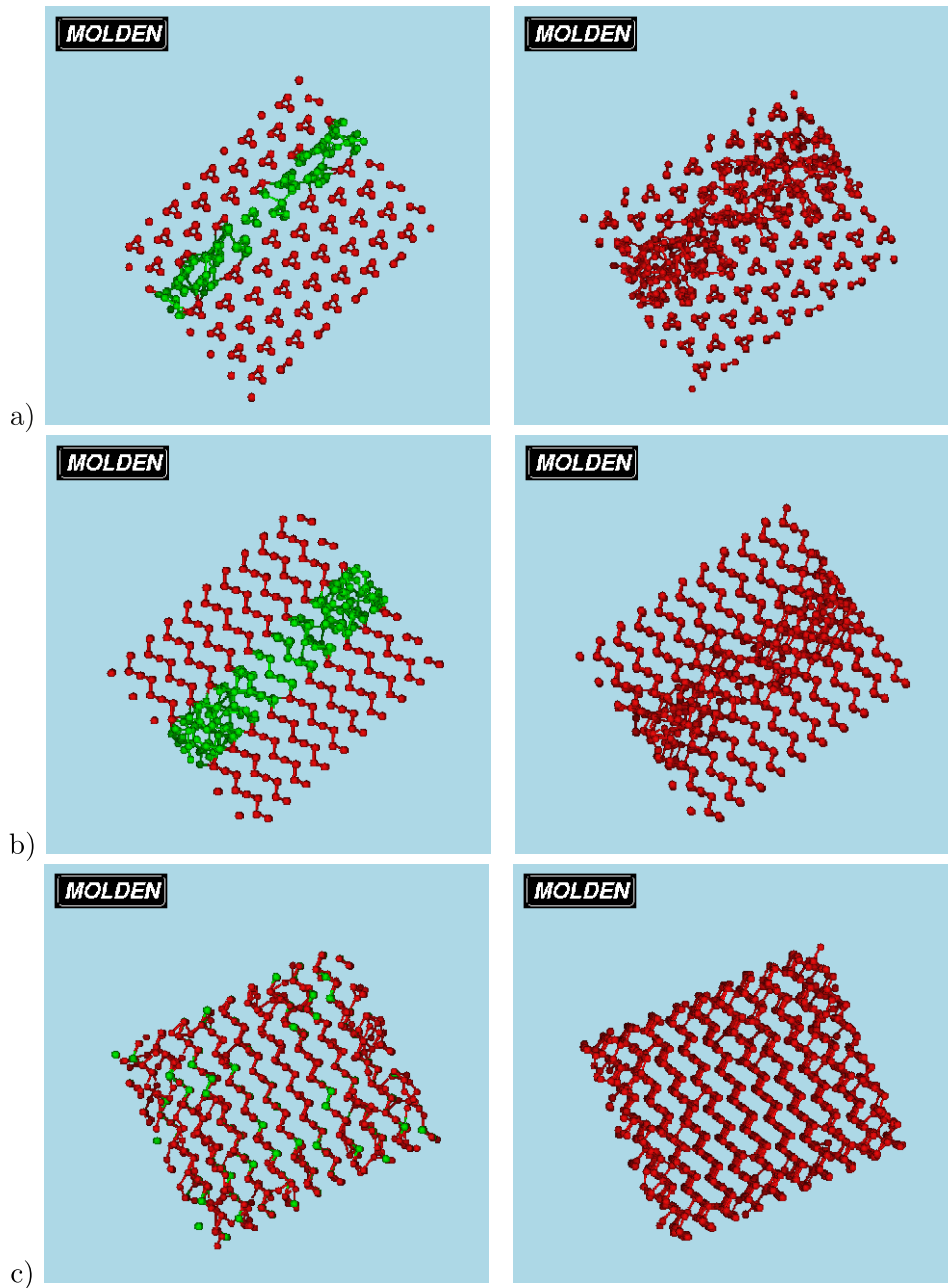
Figure 2. Disordered selenium structures by irradiating 20% of the atoms. On the left side we present configurations used as starting points for the MD simulation (atoms marked in green are shifted from their crystalline equilibrium positions, the remaining atoms are marked as red spheres). On the right side the configurations after thermal treatment and final quench are shown. (a) Disorder generated along the chains, the view is along the *c* axis, (b) disorder introduced into the plane, (c) randomly distributed disorder, the view is along the *a* axis, respectively.

for glassy selenium (see [44, 45]; we also confer with the graphs in figure 1 and the experimental results [46]). At lower degrees of disorder one can clearly observe the 'break-down' of the crystalline symmetry due to the influence of the built-in defects. The most important crystalline property of the trigonal phase is characterized by the occurrence of a double peak for the next-nearest-neighbour sphere. Using the type of amorphization within layers of helical chains this features is present in structures with up to 35% disorder, for disorder introduced within planes perpendicular to the chains, configurations with up to 65% amorphicity have this double-peak, and in randomly amorphized Se models this double peak

can still be observed at 50%. At these medium values of amorphicity one can clearly observe the anisotropic behaviour of the structures towards introduced disorder. At the lowest values of disorder, however, the crystalline peaks in the pair-correlation function can be found even at distances well beyond 10 Å. For the pair-correlation function the break-down from crystalline to amorphous behaviour will not occur at a fixed value of amorphicity; also the type of disorder is important and will have some influence on the order–disorder transition.

The vibrational densities of states calculated from the eigenfrequencies of the force constant matrix (see equation (8)) are printed in bins of width 0.04 THz and shown in
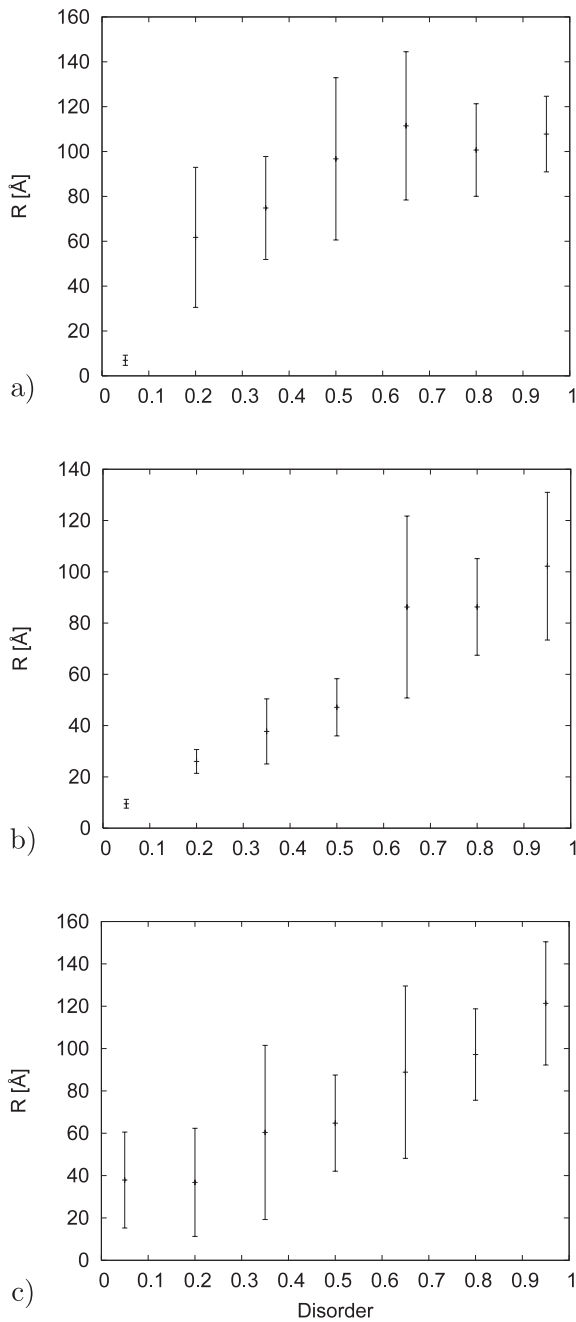
Figure 3. Total displacement R in Å of the atoms of partially disordered Se structures versus degree of disorder. The displacement is measured with respect to the crystalline reference structure. (a) Disorder introduced within the chains, (b) disorder generated in the plane, (c) randomly distributed disorder.
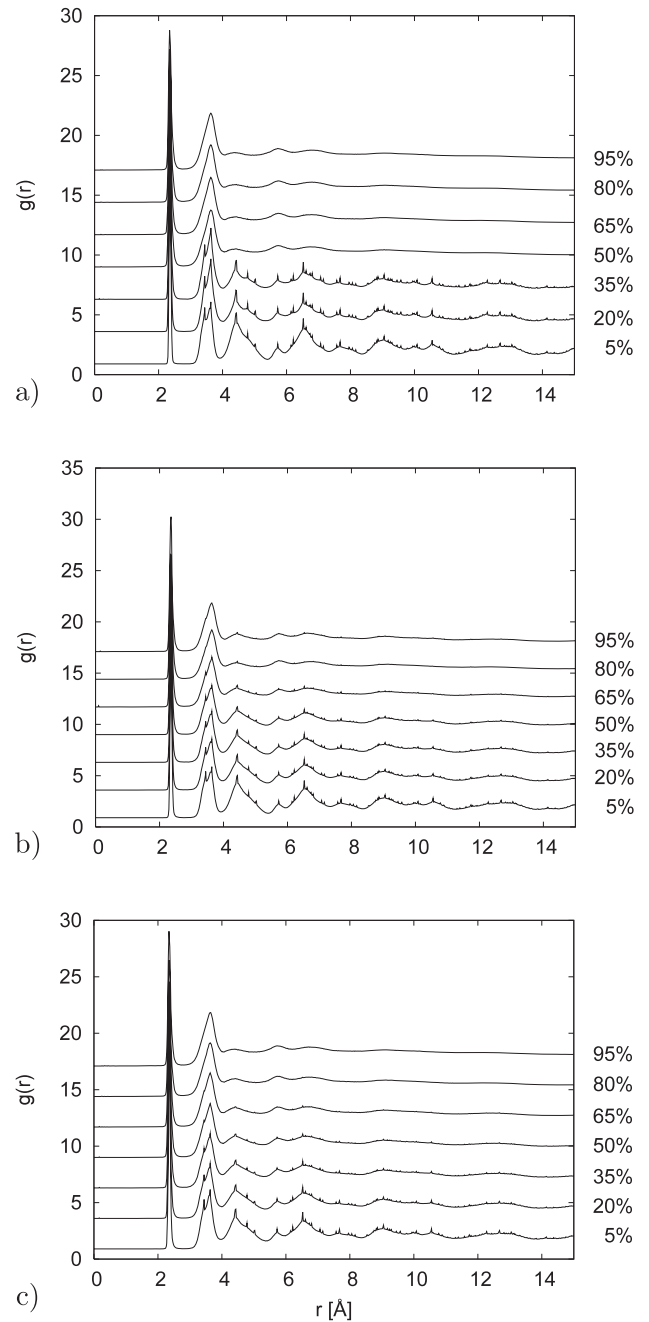

Figure 4. Pair-correlation function $g(r)$ of all degrees of amorphization for the Se structures versus distance r (Å). (a) Disorder generated along the chains, (b) disorder introduced into the plane, (c) randomly distributed disorder.

figure 5. On top of the figure (figure 5(a)) we printed the spectra of the structures with disorder introduced in layers of chains. In figure 5(b) the densities of states which are present in configurations with disordered planes are shown. In figure 5(c) the spectrum $Z(\nu)$ resulting from randomly distributed disorder is plotted. On the left of each sub-figure the corresponding degree of disorder is specified. For all types of introduced disorder we clearly observe a shift of the spectral densities to both higher and lower frequencies with increasing disorder. Since at high degrees of amorphicity ($\geqslant 65\%$) the

results of different types of disorder are very similar, one can clearly see the break-down of the crystalline structure expressed by the reduction of the peak intensity of the extended symmetric and asymmetric bond-stretching modes [51], as the high-frequency double peak vanishes in the vibrational density of states. As already seen for the pair-correlation function the vibrational density of states also depends on the types of introduced disorder. Using the type of amorphization within complete chains the high-frequency double peak is present at an amorphicity of 5%, in structures where disorder
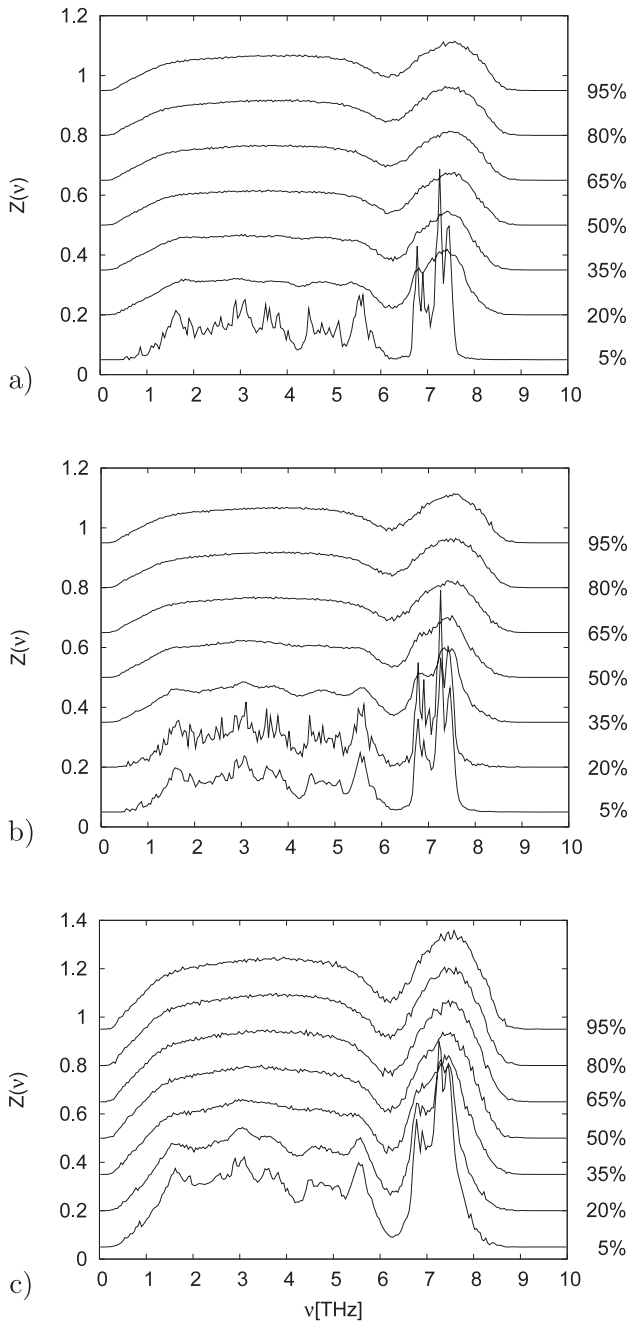
Figure 5. Frequency spectra $Z(\nu)$ of all degrees of amorphization for the disordered Se structures versus frequency ν in THz. In (a) disorder is generated along the chains, in (b) disorder is introduced into the plane and in (c) we show the results of randomly distributed disorder.

is introduced within planes perpendicular to the chains one can register this high-frequency double peak up to an amorphicity of 35%, and in randomly amorphized Se models this double peak is found at a disorder up to 20%. So we observe the same trend as for $g(r)$ that the crystalline features are best conserved in structures where disorder is only realized in planes. However, the break-down of the characteristic property will occur at different degrees of amorphization.

At low degrees of disorder the anisotropic, i.e. helical, structure of the trigonal Se crystal is still present. Its influence

on the vibrations, and especially on the localization or better the extension of the eigenmodes, can be seen in the density of states and is well established by the presence of the above-mentioned high-frequency double peak. The participation ratio (see equation (12)) and the effective mass as $n_{\mathrm{eff}} = m_{\mathrm{eff}}/m$ (see equation (11)) are well-established quantities to measure the localization or, vice versa, the extension of a vibrational mode. In figure 6 the resulting values of the participation ratios (on the left of the figure) and the effective masses (on the right) are plotted versus frequency. Part (a) of figure 6 displays—as usual—the results obtained for structures with disordered layers of chains. In figure 6(b) both the participation ratio and the effective mass are depicted from configurations with disordered planes. In figure 6(c) we give the values obtained from randomly disordered material. In each graph the individual lines represent the results of increasing disorder from 5% to 95% (bottom up). As shown in figure 6 the disorder (up to 50%) introduced in planes perpendicular to the chains does not have much influence on the extension of the high-frequency modes, whereas for the other types of introducing disorder the break-down of the extension of the eigenmodes and the localization at higher frequencies can already been seen at 20% disorder. The localization of modes (glass-like structures) is an important sign for the break-down of symmetry, which, vice versa, gives hints to the disorder of matter.

Since the shifts of the trigonal reference frequencies can already be seen qualitatively in figure 5 we would now give a closer and more quantitative look at these shifts. Using equation (10) as a measure to quantify shifts in both directions (i.e. to either lower or higher frequencies) we calculated $(\Delta \nu)^2$ for all 210 structures, with the trigonal spectrum being the reference. In figure 7 we show our results for the shifts of the frequencies versus the degree of amorphicity. Again we split the figure into three parts to distinguish between the different types of disorder. In figure 7(a) we show the frequency shifts obtained for structures with disordered chains. In part (b) of figure 7 the results are shown for those configurations with irradiated planes. At the bottom of the plot, figure 7(c), we give the values from randomly amorphized material. For the highest degrees of disorder (from 65% upwards) the values of the shifts are independent from the kind of introduced disorder and $\Delta \nu^2$ is about 0.08–0.09 (THz^2). For the lowest degrees of amorphicity we find a linear increase of the shifts in frequencies, best expressed for the disorder introduced within planes perpendicular to the chains.

4. Discussion

The focus of our simulation is mainly laid on structural properties and dynamics, i.e. vibrational properties of selenium, which are prepared using different degrees of amorphization, namely nearly perfect crystalline, partially crystalline, partially disordered and fully amorphous structures. With respect to the anisotropy of the trigonal phase we also considered three types of introducing defects and disorder into the configurations. Groups of atoms, which comprise layers of complete chains, or which belong to planes perpendicular to the prominent
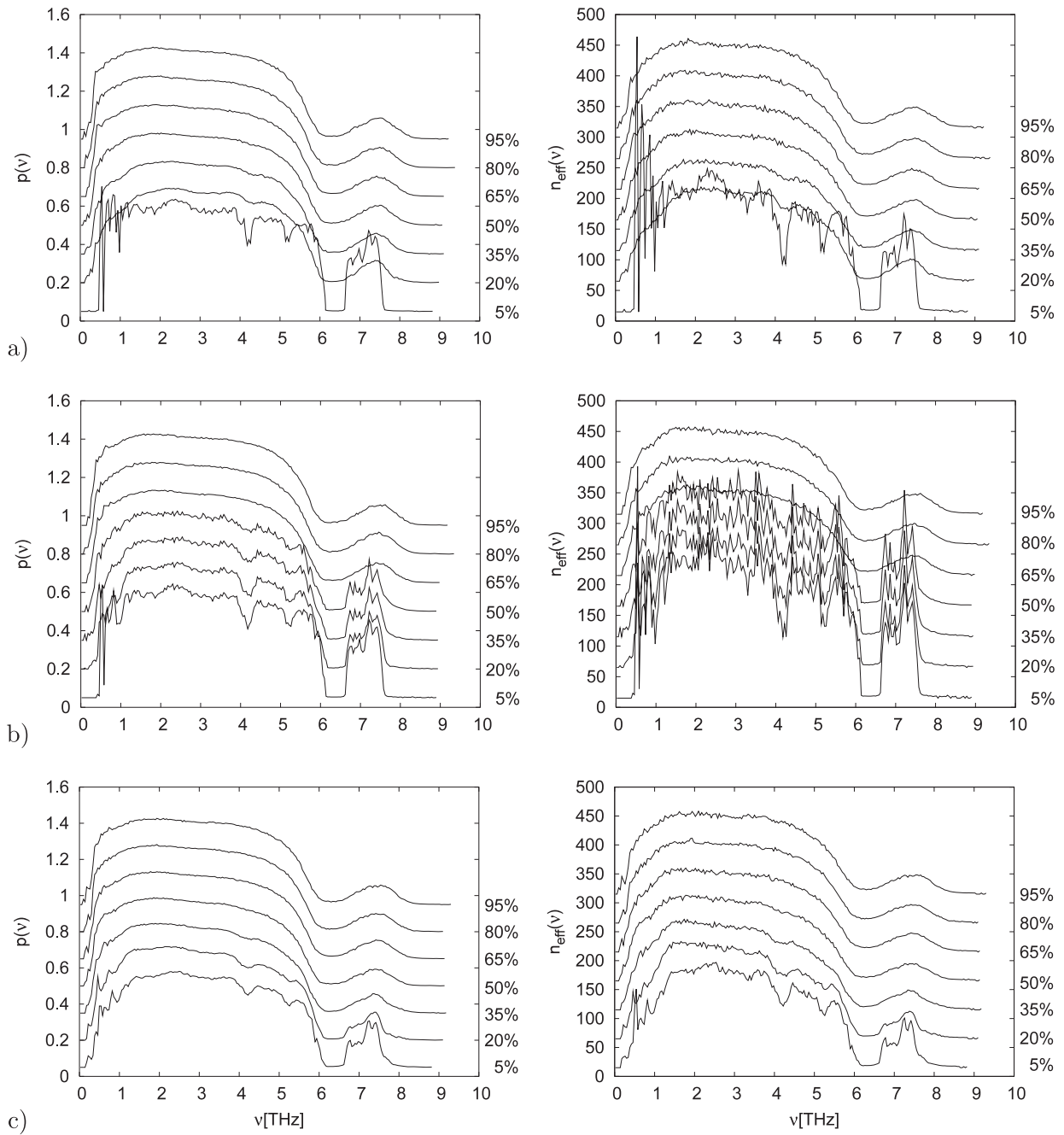
Figure 6. For all degrees of amorphization of the disordered Se structures we plot the participation ratio $p(\nu)$ (left) and the effective mass as $n_{\mathrm{eff}}(\nu) = m_{\mathrm{eff}}/m$ (right) versus frequency ν in THz. (a) Disorder generated along the chains, (b) disorder introduced into the plane, (c) randomly distributed disorder.

chains, or which are randomly chosen, are displaced from their equilibrium positions.

As can be deduced from figure 2 there is a remarkable difference in the types of disorder at a low degree of amorphicity. If one introduces disorder within planes perpendicular to the helical chains the disorder will not spread to such an extent if one randomizes atoms of layers within the chains. This is a strong hint towards differences between inter- and intra-molecular coupling (i.e. coupling between atoms of different chains or atoms within the same chain, respectively). Despite the fact that we do not make any

distinction in the interaction potential (cf equations (1), (2) and (4)), the system reacts anisotropically, which, vice versa, leads to the conclusion that the observed effects are structurally inherent. The selenium model exhibits a stronger coupling between adjacent chains compared to the coupling between neighbouring atoms within the same chain. As long as the chain structure is present for low degrees of disorder, the atoms of one chain possess four next-nearest neighbours in three adjacent chains (d_{nn} = 3.44 Å), whereas only two next-nearest neighbours are present within the same chain (d_{nn} = 3.63 Å). Due to that reason, the disorder can be easily
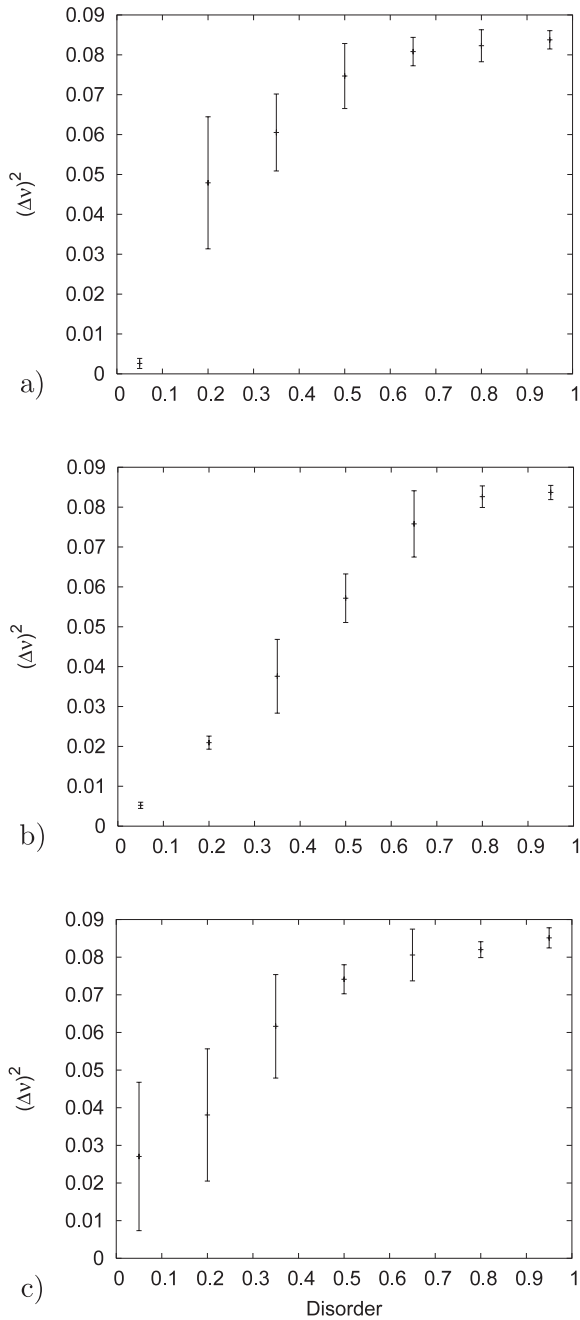
Figure 7. Total shift $(\Delta\nu)^2$ of the frequencies of partially disordered Se structures versus the degree of disorder. (a) Disorder introduced within the chains, (b) disorder generated in the plane, (c) randomly distributed disorder.

transported through the coupling between the chains and will affect and influence the close vicinity of the chains. In contrast to this, layers of neighbouring planes are less affected by the introduced disorder, since their coupling is weaker compared to the chains, in a sense that due to a smaller number of neighbouring atoms (compared to the numbers of next-nearest atoms from adjacent chains) the relaxation of local energy spots caused by disorder is reduced.

If one assumes the total distance R being a measure for the 'conservation' of a structure and, furthermore, if one assumes that a complete loss of the crystalline memory is reached if every atom is displaced by roughly one nearest-neighbour

distance from its starting equilibrium position (as a rule of thumb), we could estimate that this assumption corresponds to a total displacement $R \approx 88$ Å for our system. From figure 3 we see that this criterion is fulfilled if the structure is distorted by 50% within the chains: however, for other types of disorder, 65% of displaced atoms are needed to get a total displacement of about $R \approx 88$ Å.

Comparison of the pair-correlation function being a main indicator of structural disorder exhibits in all cases a strong first peak, which proves the chemical short-range order to be present in solids, which can be clearly found in figure 4. The so-called *nearest-neighbour peak* describes the first coordination sphere around a reference atom. The increasing disorder and hence the amorphization is revealed by reduced intensities of the peaks and increasing the full width at half-maximum (FWHM). The influence of the disorder can be seen clearly at the next-nearest-neighbour coordination sphere, which is split into two peaks in a crystalline-like structure. The first maximum of the double peak results from the next-nearest-neighbour distance of atoms of different chains (inter-chain distance $r_{nn} = 3.44$ Å to four atoms) and the second maximum is caused by the distance of next-nearest neighbours within one chain (intra-chain distance $r_{nn} = 3.63$ Å to two atoms) [52]. In glasses the double-peak structure of the next-nearest-neighbour peak is not found and only one peak at $r_{nn} = 3.63$ Å, similar to the intra-chain distance, exists. This is a strong hint to the fact that in disordered Se the chains have been broken and rings have been formed during the melting process, which has been confirmed by both simulations [53, 54] and experiments [55, 56].

Figure 5 shows the vibrational density of states as $Z(\nu)$ averaged over all configurations: for the highest degree of disorder, we find an equivalent $Z(\nu)$ as in glasses [57]. One sees a clear enhancement of the glassy spectrum at low frequencies which reaches well beyond frequencies where system sizes could be of importance. A shortcoming of the interaction potential is that the experimentally observed double peak at high frequencies cannot be reproduced. In the low-frequency part the spectrum is shifted to lower frequencies compared to experiment [47] which also has a strong impact on dynamic properties since in the model the sound velocities are too high compared to experiment [48] as well as the specific heat is too low [49, 50]. These findings are in agreement with earlier simulations which have their focus on temperature effects on the spectral density of states [51]. As mentioned in section 2 the localization of the eigenmodes is a good criterion for the special behaviour concerning dynamic and thermodynamic properties of amorphous materials or glasses. Since the localization of modes, i.e. dynamic is hindered to spread over the structure, causes a reduction of the transport properties, the presence of local eigenmodes leads to reduced heat transfer. In figure 6 the participation ratios and the effective masses for the three amorphization types clearly give insight into the anisotropy of the Se structures. Structures with disorder introduced in planes are much more 'stable' with respect to crystallinity, since the extension of eigenmodes holds at least up to an amorphicity of 50%, whereas for the other types of disorder (introduced randomly or within

the chains) an amorphicity of 20% is sufficient to break the extension of the modes.

In contrast to a different class of material, namely the tetrahedrally bonded structures (e.g. zeolite ZSM-5-based amorphous material [61] where the spectrum is completely shifted towards lower frequency), we observe for the trigonal Se-based amorphized structures a broadening of the spectrum. Figure 7 shows this behaviour for the differently prepared states of Se structures. For higher degrees of amorphization (⩾65%) the shifts do not depend on the preparation and, on average, the square of the frequency shift corresponds to a value of about 0.08 THz^2 per mode. However, for low degrees of disorder small frequency shifts occur, which can be explained by anharmonic effects of the atomic interactions, which play a crucial role in disordered or distorted structures (or parts of structures). At the lower-frequency part of the spectrum the frequencies are shifted towards even lower values—with increasing disorder. This observation is in agreement with the fact that in disordered materials low-frequency excess modes exist (a fact which is an explanation for the low temperature anomalies). With increasing disorder the high-frequency part of the vibrational density is losing its characteristic double-peak structure and is broadened. This effect is a direct consequence of the influence due to structural defects or due to disorder. Since in different surroundings or environments the vibrational (here symmetric and asymmetric stretching) modes will (slightly) change their frequencies, their overlap leads to broadening of the single peaks and characteristic features are 'wiped out'. Having a closer look at the number of modes which are shifted to lower frequencies and those shifted to higher values of the spectrum, we find that for highly disordered structures about 65% of the modes are shifted towards lower frequencies.

5. Summary and conclusion

Introducing different degrees of amorphicity into a trigonal Se crystal (comprising $N = 1470$ atoms) we simulated structural and dynamic properties using molecular dynamics techniques. Amorphicity is generated by shifting atoms from their crystalline equilibrium positions: the numbers of shifted atoms correspond to 5%, 20%, 35%, 50%, 65%, 80% and 95% of the complete structure. For each degree of disorder ten configurations are simulated and aged for 17.6 ps at 140 K.

For high degrees of disorder our results concerning both structural and dynamic properties resemble those for the classical melting route: however, the proposed type of irradiation is computationally faster to perform compared to the classical melting process. The results of Se structures generated using a classical melting route [58], compared to those obtained via irradiation strategies, show good and reasonable agreement, so we have presented an acceptable alternative with our irradiation strategy to simulate the properties of disordered materials, which could also be interpreted as good representatives for glassy material, at least for some static and dynamic ($g(r)$ and $Z(\nu)$, respectively) properties.

For the lowest degrees of amorphicity (⩽20%) the obtained results give important insights into the anisotropic behaviour of generated structures and underlying dynamic processes. For very low disorder the pair-correlation functions $g(r)$ show crystalline features, especially the pronounced double-peak structure in the next-nearest-neighbour shell. With increasing disorder we observe a broadening of the nearest-neighbour shell: however, the chemical short-range order is conserved through all stages of the solid state. Break-down of crystallinity is connected with the breakage of the chains and their hexagonal alignment which causes a peak in the second-neighbour shell at a distance $d_{nn} = 3.44$ Å. The reduction and loss of that peak is a sign for the breaking of chains and for the re-building of the structure, i.e. formation of short disordered chains and rings, which, vice versa, leads to a uniform next-nearest-neighbour peak with a distance at $d_{nn} = 3.63$ Å, caused by next-nearest neighbours within a chain or ring. The transition from crystalline to amorphous states does not take place at a fixed degree of disorder. It is strongly influenced by the type of disorder present in the structure.

The frequency spectra clearly exhibit the influence of the amorphization or the disorder introduced into the structure, and crystalline properties will be established as well as the anisotropy of the chain-like structural building unit. The main features of the trigonal phase are the chains, and as long as these are not drastically irritated the crystalline character of the properties are conserved best. As long as the disorder is spread perpendicular to the chains the chain-like character is present, so introducing disorder within complete chains or randomly will have a stronger impact on the symmetry. This has also great influence on dynamic properties (as can be seen in the shift of the values of frequencies and in the extension of the eigenmodes) which in course will affect thermodynamic properties (heat transport and specific heat).

Increasing the degrees of irradiation one can clearly see a shift of the frequencies to both lower (at the low-frequency part) and higher (at the high-frequency part) values, i.e. the spectrum is broadened by disorder. In amorphous Se (similar to Se glasses) the shift of modes towards lower frequencies causes so-called excess modes, which are responsible for the anomalous low temperature behaviour [59]; in particular the specific heat is strongly influenced by these localized low-frequency modes [60]. The distinguished peak (especially in the high-frequency part of the spectrum, caused by symmetric and asymmetric bond-stretching modes) of the crystalline material will be reduced and broadened with increasing amorphicity. The energy gap between the high-frequency and low-frequency region (typical for the trigonal structure) will be drastically suppressed at 35% for all types of amorphization.

Looking at the most important dynamic and structural properties, the loss of crystallinity depends on the type of disorder: however, for the pair-correlation function $g(r)$ this effect is shifted to higher degrees of amorphization compared to the density of states $Z(\nu)$. This leads to the conclusion that dynamic properties are more sensitive to the influences caused by (structural) disorder or defects than the structural properties are.

References

[1] Phillips W A 1972 *J. Low Temp. Phys.* **7** 351
[2] Vashishta P, Kalia R K, Nakano A, Homan B E and McNesby K L 2007 *J. Propuls. Power* **23** 688
[3] Qi Y, Strachan R, Cagin T and Goddard W A III 2001 *Mater. Sci. Eng.* A **309** 156
[4] Duan Y and Kollman P A 1998 *Science* **282** 740
[5] Duwez P, Willens R H and Klement W Jr 1960 *J. Appl. Phys.* **31** 1136
[6] Hegedüs J, Kohary K and Kugler S 2004 *J. Non-Cryst. Solids* **338–340** 283
[7] Zarzycki J 1991 *Materials Science and Technologies* vol 9, ed R W Cahn, P Haasen and E J Kramer (Weinheim: VCH)
[8] Basu Mukhopadhyay A, Oligschleger C and Dolg M 2004 *Phys. Rev.* B **69** 12202
[9] Schober H R, Gaukel C and Oligschleger C 1997 *Defect Diffus. Forum* **143–147** 723
Schober H R, Gaukel C and Oligschleger C 1997 *Prog. Theor. Phys. (Kyoto)* **126** 67
[10] Oligschleger C, Gaukel C and Schober H R 1999 *J. Non-Cryst. Solids* **250–252** 660
[11] Oligschleger C and Schober H R 1999 *Phys. Rev.* B **59** 811
[12] Cherin P and Unger P 1972 *Acta Crystallogr.* B **28** 31
[13] Donohue J 1974 *The Structures of the Elements* (New York: Wiley)
[14] Miyamoto Y 1980 *Japan. J. Appl. Phys.* **19** 1813
[15] Phillips W A, Buchenau U, Nücker N, Dianoux A J and Petry W 1989 *Phys. Rev. Lett.* **63** 2381
[16] Lasjaunias J C, Maynard R and Thoulouze D 1972 *Solid State Commun.* **10** 215
[17] Buchenau U, Galperin Yu M, Gurevich V L and Schober H R 1991 *Phys. Rev.* B **43** 5039
[18] Oligschleger C, Jones R O, Reimann S M and Schober H R 1996 *Phys. Rev.* B **53** 6165
[19] Stillinger F H, Weber T A and La Violette R A 1986 *J. Chem. Phys.* **85** 6460
Stillinger F H and Weber T A 1987 *J. Phys. Chem.* **91** 4899
[20] Berkowitz J and Chupka W A 1966 *J. Chem. Phys.* **45** 4289
[21] Bondybey V E and English J H 1980 *J. Chem. Phys.* **72** 6479
[22] Schnöckel H, Göcke H-J and Elsper R 1982 *Z. Anorg. Allg. Chem.* **494** 78–86
[23] Hoareau A, Reymond J-M, Cabaud B and Uzan R 1975 *J. Physique* **36** 737
[24] Car R and Parrinello M 1985 *Phys. Rev. Lett.* **55** 2471
[25] Jones R O 1986 *J. Chem. Phys.* **84** 318
[26] Hohl D, Jones R O, Car R and Parrinello M 1987 *Chem. Phys. Lett.* **139** 540
[27] Hohl D and Jones R O 1991 *Phys. Rev.* B **43** 3856
[28] Hultgren R, Desai P D and Hawkins D T (ed) 1973 *Selected Values of the Thermodynamic Properties of the Elements* (Metals Park, Ohio: American Society for Metals)
[29] Mills K C 1974 *Thermodynamic Data for Inorganic Sulphides, Selenides and Tellurides* (London: Butterworth)
[30] Mooradian A and Wright G B 1969 *The Physics of Selenium and Tellurium* ed W Ch Cooper (London: Pergamon)
[31] Lucovsky G 1969 *The Physics of Selenium and Tellurium* ed W Ch Cooper (London: Pergamon)
Lucovsky G, Mooradian A, Taylor W, Wright G B and Keezer R C 1967 *Solid State Commun.* **5** 113
[32] Cicotti G, Frenkel D and McDonald I R (ed) 1987 *Simulations of Liquids and Solids* (Amsterdam: North-Holland)
[33] Allen M P and Tildesley D J 1987 *Computer Simulation of Liquids* (Oxford: Clarendon)
[34] Hansen P and McDonald I R 1976 *Theory of Simple Liquids* (New York: Academic)
[35] Heermann D W 1990 *Computer Simulation Methods* (Berlin: Springer)
[36] Nosé S and Klein M L 1983 *Mol. Phys.* **50** 1055
[37] Dickey J H and Paskin A 1969 *Phys. Rev.* **188** 1407
[38] Beeman D and Alben R 1977 *Adv. Phys.* **26** 339
[39] Harwell Subroutine Library, AERE Harwell, Didcot, UK
[40] Fletcher R and Reeves C M 1964 *Comput. J.* **7** 149
[41] Maradudin A A, Montroll E W, Weiss G H and Ipatova I P 1971 *Theory of Lattice Dynamics in the Harmonic Approximation, Solid State Physics* Supplement 3 (New York: Academic)
[42] Smith B T, Boyle J M, Dongarra J J, Garbow B S, Ikebe Y, Klema V C and C B Moler 1976 *Matrix Eigensystem Routines—EISPACK Guide* (Berlin: Springer)
[43] Cochran W 1973 *The Dynamics of Atoms in Crystals* (London: Arnold)
[44] Oligschleger C and Schober H R 1995 *Solid State Commun.* **93** 1031
[45] Bichara C, Pellegatti A and Gaspard J-P 1994 *Phys. Rev.* B **49** 6581
[46] Needham L M, Cutroni M, Dianoux A J and Rosenberg H M 1993 *J. Phys.: Condens. Matter* **5** 637
[47] Gompf F 1981 *J. Phys. Chem. Solids* **42** 539
[48] Meißner M and Mimkes J 1979 *Physics of Selenium and Tellurium* ed E Gerlach and P Grosse (Berlin: Springer)
[49] Kugler H K (ed) 1981 *Gmelin Handbuch der Anorganischen Chemie* (Berlin: Springer)
[50] Gaur U, Shu H-C, Mehta A and Wunderlich B 1981 *J. Phys. Chem. Ref. Data* **10** 89
[51] Oligschleger C and Schön J C 1997 *J. Phys.: Condens. Matter* **9** 1049
[52] Wyckoff R G W 1982 *Crystal Structures* (Florida: Krieger)
[53] Oligschleger C and Schober H R 1999 *J. Non-Cryst. Solids* **250–252** 651
[54] Hohl D and Jones R O 1991 *Phys. Rev.* B **43** 3856
[55] Lucovsky G and Wong C K 1985 *J. Non-Cryst. Phys.* **75** 51
[56] Carrol P J and Lannin J S 1981 *Solid State Commun.* **40** 81
[57] Schober H R, Oligschleger C and Laird B B 1993 *J. Non-Cryst. Solids* **156–158** 965
[58] Oligschleger C and Schober H R 1993 *Physica* A **201** 391
[59] Zeller R C and Pohl R O 1971 *Phys. Rev.* B **4** 2029
[60] Schober H R and Oligschleger C 1996 *Phys. Rev.* B **53** 11469
[61] Mukhopadhyay A B, Oligschleger C and Dolg M 2003 *Phys. Rev.* B **68** 24205